Check for updates

# The shell microstructure of the pteropod *Creseis acicula* is composed of nested arrays of S-shaped aragonite fibers: A unique biological material

Odelia Sibony-Nevo, Katya Rechav, Viviana Farstey, Eyal Shimoni, Neta Varsano, Lia Addadi, and Steve Weiner*

Snails of the superfamily Cavolinioidea, known as pteropods, are very abundant in the surface waters of all the oceans. Their transparent and lightweight shells are composed of densely packed, well-aligned, continuously crystalline curved aragonite fibers. Previous studies of the shell microstructure using mainly scanning electron microscopy, transmission electron microscopy, and x-ray diffraction suggested that the aragonite fibers adopt a helical motif. We mainly used focused ion beam-scanning electron microscopy to obtain three-dimensional information on the shell structure of *Creseis acicula.* We show that the basic structural motif in the central part of the shell (teleoconch) comprises aragonite fibers that are not helical, but are organized in nested S-shaped arcs arranged in planar arrays. This plane is oblique to the outer shell surface by approximately 20°. The planes stack in the third dimension with local displacements, to form a unique biological material.

## Impact statement

Of the seven basic materials used by mollusks to build their shells, the structure of one of these materials remains enigmatic, even though the snails that form this structure are by far the most abundant mollusks on earth. These so-called pteropods live in the surface waters of all the oceans and produce a significant amount of all the calcium carbonate formed in the open oceans. Since the first study of the pteropod shell structure in 1972, the basic structural motif of the arrays of highly elongated aragonite crystal fibers was inferred to be helical, although no one actually documented an entire helix. Here we resolved the 3D structure of the shell of one pteropod species using an instrument (FIB-SEM) that produces a high resolution 3D structure. We show that the basic repeating unit is a planar layer of nested S-shaped aragonite crystal fibers. Furthermore this planar layer is oblique to the shell outer surface. Besides resolving a fundamental basic question concerning mollusk shell structures, this unique organization of crystals raises fascinating questions about the mechanical properties of this most unusual curved space filling structure that will hopefully inspire materials scientists to produce superior synthetic materials.

## Introduction

The mollusks produce seven different types of shell materials.[1–3] The structures of six of these materials are relatively well documented.[2,4] The seventh material is present in only two molluscan groups; the Cavolinioidea superfamily of pteropods[5,6] and the Atlantidae family of pterotracheoids (heteropods).[7] The pteropods live in the upper 1000 m of the oceans, but most species are found close to the ocean surface (up to a depth of 200 m).[6,8]

Two superfamilies belong to the shelled pteropods (Euthecosomata): The Limacinoidea and Cavolinioidea. The shells of both superfamilies are composed of aragonite, but their shell shapes and microstructures are

Odelia Sibony-Nevo, Department of Structural Biology, Weizmann Institute of Science, Israel; Odelia.sibony@weizmann.ac.il
Katya Rechav, Department of Chemical Research Support, Weizmann Institute of Science, Israel; katya.rechav@weizmann.ac.il
Viviana Farstey, The Interuniversity Institute for Marine Sciences, Israel; viviana.farstey@mail.huji.ac.il
Eyal Shimoni, Department of Chemical Research Support, Weizmann Institute of Science, Israel; Eyal.Shimoni@weizmann.ac.il
Neta Varsano, Department of Structural Biology, Weizmann Institute of Science, Israel; neta.varsano@gmail.com
Lia Addadi, Department of Structural Biology, Weizmann Institute of Science, Israel; Lia.Addadi@weizmann.ac.il
Steve Weiner, Department of Structural Biology, Weizmann Institute of Science, Israel; Steve.Weiner@weizmann.ac.il
*Corresponding author

different. The Limacinoidea shells are coiled in a manner similar to other gastropods, whereas the shells of the Cavolinioidea are uncoiled and are bilaterally symmetrical.[9] The Limacinoidea coiled shell is composed of the most common microstructure produced by gastropods, namely the crossed lamellar microstructure.[8,10,11] The building blocks of the crossed lamellar structure are very small elongated crystals of aragonite with rectangular cross sections about 0.2-μm wide.[12] On the other hand, the building blocks of the bulk of the Cavolinioidea shells comprise highly elongated and curved crystals of aragonite that have roughly the same cross sectional dimensions as the crystals in the crossed lamellar structure (around 0.2–0.3 μm).[8,13–15] Bé et al.[8] showed that the shell is composed of a thin outer prismatic layer and an underlying much thicker helical microstructure. Bé et al.[8] also showed that pteropods from the Cavolinioidea superfamily increase their length by shell deposition at the forming edge and that the animal thickens its shell throughout its life. New mineral is deposited via a disordered precursor phase.[15]

Zhang et al.[16] studied the shell microstructure of *Cavolinia uncinata* and also concluded that the densely packed nanofibers form a helix. The irregular, but somewhat rectangular cross sections of the fibers form an interlocked mosaic microstructure. Mechanical examination of the shell by nanoindentation shows that the elastic modulus is anisotropic. In a section transverse to the shell thickness the modulus is $85.9\pm2.7$ GPa, whereas in the plane of the natural surface the modulus is $51.5\pm1.6$ GPa. This is attributed to the densely packed helical nanofiber structure.

Li et al.[14] studied the hierarchical structure and mechanical design of *Clio pyramidata*. They too concluded that the densely packed curved aragonite fibers have a helical structure. The shell thickness varies from 20 to 200 μm with an increase in the number of turns as the shell thickens. Transmission electron microscopy (TEM) characterization of the nanofiber cross section confirmed the interlocking mosaic microstructure and Li et al.[14] identified the presence of organic inclusions within the fibers. They also noted that the fibers have a non-uniform cross section. Microindentation and electron microscopy showed that the helical organization of the fibrous building blocks effectively limits mechanical damage by ensuring tortuous crack propagation.

The shell microstructure of *Cuvierina columnella* was studied by Checa et al.[17] and Willinger et al.[18] Adjacent curved crystal fibers can intersect each other and even cross each other to form an interlocking structure.[17] The aragonite fibers protrude from the forming surface at a low angle.[6,18] Willinger et al.[18] showed that the fibers are continuously crystalline, and have a preferred crystallographic growth direction along the aragonite *b*-axis. Others have concluded that there is a significant spread of the aragonite *a*- and *b*-axes directions,[13,14] although all agree that the crystal *c*-axes are more or less perpendicular to the shell surface.[13,14,16,18] Willinger et al.[18] hypothesized that recurrent twinning enables the fibers to curve, but still remain as single crystals that elongate along the *b*-axis direction. Willinger et al.[18] also showed that the helical plane is tilted by about 20° from the shell surface.

Suzuki et al.[13] inferred the presence of the helical microstructure from fracture surfaces through the shell thickness. They proposed that the fiber is composed of 1–2 μm long single crystals of aragonite that change orientation as the fiber curves. The helical plane is tilted by about 15° to the shell surface.

We note that in all the above studies curved crystal fiber arrays are observed, and following Bé et al.'s original proposal all these studies assume that the structure is helical. In none of these studies was a complete helix documented. Furthermore, it is conceptually difficult to conceive how a helical structure can be space filling, and no major pores have been documented in the shell structure. In this study, we use focused ion beam coupled with scanning electron microscope imaging (FIB-SEM) to document the 3D structure of the shell of *Creseis acicula* (previously known as *Creseis clava*[19]).

## Materials and Methods

### Animals
Living specimens of *Creseis acicula* larvae (veliger) and adult individuals were collected in Eilat, the Red Sea, as described by Sibony-Nevo et al.[15] Some of the living specimens were preserved in 70% or 100% ethanol, whereas other specimens were immersed in filtered sea water containing 10% dextran (Fluka), used as a cryoprotectant, and then high pressure frozen for further examination in the SEM and FIB-SEM.

### SEM of the shell
The *C. acicula* shells were prepared and imaged on SEM as described by Sibony-Nevo et al.[15] The specimens preserved in 100% ethanol, were dried and their shells were broken with a scalpel to reveal different sections of the shell. These shell pieces were mounted on an aluminum stub with double-sided carbon tape. High resolution images were obtained using a Leo-Supra 55 VP FEG SEM or an Ultra 55 SEM (Carl Zeiss Microscopy GmbH, Oberkochen, Germany).

### X-Ray diffraction
Dry shells of adult *C. acicula* were cut in half and mounted on glass fibers with Superglue. Diffraction patterns were collected with a Rigaku MX007HF rotating anode equipped with Osmic VHF optics. The shell was exposed to the x-ray beam perpendicular and then parallel (i.e., at φ=0, 90, 180, and 270°) to the external shell surface in different regions of the shell. Cu Kα1 radiation was used with a beam size of 100 μm. The shell was moved back and forth by 0.5° between each frame. Irradiation was performed at room temperature.

### FIB-SEM
#### Sample preparation
For stained samples, living specimens of adult *C. acicula* were immersed in filtered sea water containing the cryoprotectant

**Table I. Serial surface view (SSV) stacks (St) obtained from two specimens of *C. acicula*.**

| Stack | Stained/Unstained | Volume (μm) | Voxel Size (nm) | Microscope | Location |
|-------|-------------------|-------------|-----------------|------------|----------|
| St A | Stained | $X=20, Y=17, Z=17$ | 10 nm × 10 nm × 50 nm | Helios Nanolab 600 | Teleoconch |
| St B | Stained | $X=40, Y=35, Z=9$ | 10 nm × 10 nm × 20 nm | Helios Nanolab 600 | Teleoconch |
| St C | Stained | $X=40, Y=35, Z=4.5$ | 9 nm × 9 nm × 10 nm | Helios Nanolab 600 | Protoconch |
| St D | Stained | $X=40, Y=35, Z=18$ | 10 nm × 10 nm × 10 nm | Helios Nanolab 600 | Protoconch |
| St E | Stained | $X=44, Y=35, Z=40$ | 9 nm × 9 nm × 18 nm | Zeiss Crossbeam 550 | Teleoconch (Close to growing edge) |
| St F | Not stained | $X=40, Y=35, Z=0.6$ | 10 nm × 10 nm × 20 nm | Helios Nanolab 600 | Teleoconch |
| St G | Stained | $X=25, Y=15, Z=5.5$ | 10.5 nm × 10.5 nm × 10 nm | Zeiss Crossbeam 550 | Teleoconch |

The parameters for each stack specify whether the sample was stained or not, the stack volume (μm), voxel size (nm), the FIB-SEM used, and the location on the shell chosen for imaging. See Figure 1 for the definition of protoconch and teleoconch in *C. acicula*.

10% dextran (Fluka). The samples were then sandwiched between two metal discs (3 mm diameter and 0.05, 0.1 or 0.15 mm cavities depending on the specimen thickness). The samples were cryo-immobilized in a high pressure freezing device (HPM10; Bal-Tec, Liechtenstein) and were kept in liquid nitrogen, then freeze-substituted (EM AFS2, Leica Microsystems, Vienna, Austria) in 2% glutaraldehyde and 1.5% $OsO_4$ in absolute acetone. The sample temperature was then raised progressively from −90 to −30°C over 44 h. After an additional 24 h, 1% uranyl acetate in acetone was added to the samples after washing with acetone at −30°C. Samples reached 0°C in 20 min, and were kept for 2.5 h at room temperature with uranyl acetate and later washed with acetone. After removal of the water, the fixed samples were embedded in Epon (Agar Scientific, UK) and polymerized at 60°C. The samples were cut longitudinally with an Ultracut UCT microtome (Leica Microsystems, Wetzlar, Germany). Unstained samples were prepared from living animals immersed in 100% ethanol, air dried, and embedded following the same procedure that was performed on stained samples.

In both stained and unstained samples, the Epon embedding was carried out in the following steps: 20%, 30%, and 40% Epon in acetone for 2 h on a rotor, 50%, 60%, and 70% Epon for 4 h, 80% Epon for 5 h, 90% Epon for 9 h, and 100% Epon three times for 12 h. Finally, each sample was put in a drop of Epon and dried at 60°C. The sample was trimmed and mounted on top of empty labeled Epon blocks using a drop of non-cured Epon. In these last two steps, the sample was repositioned in the mold such that it was aligned as well as possible with the sample long axis. The longitudinal surface of the sample was exposed by trimming with a glass knife using a microtome (Leica Microsystems, Vienna, Austria). Once the longitudinal section was exposed, a diamond knife was used for polishing (Diatome AG, Biel, Switzerland). The trimmed sample was placed in a clamp holder and wrapped in carbon tape. We obtained one sample of stained and one of unstained specimens of adult *C. acicula*.

*FIB-SEM volume imaging*

Serial surface imaging, (or serial surface view (SSV)) was performed using either the Helios Nanolab 600 FIB-SEM (Thermo Fisher Scientific, OR US) or the Zeiss Crossbeam 550 FIB-SEM (Zeiss Microscopy GmbH, Oberkochen, Germany). All experiments were carried out on embedded samples, coated with a carbon evaporated conductive layer of ~10 nm. Seven stacks were obtained from two specimens (**Table I**). All the stacks essentially showed the same results. Here we present the results from Stacks B, E, and G.

In order to avoid beam damage to the surface of the sample, a 0.5-μm thick protective patch of platinum was deposited above the area of interest prior to SSV acquisition, using ion beam induced CVD at 30 keV, 700pA. A 25-μm long and 35-μm wide trench was milled just in front of the area of interest at 20 nA. Polishing of the exposed surface and serial slicing were performed using a lower ion beam current of 0.7nA.

SEM images were collected at 3–3.2 keV, 350–650 pA using the automated "Slice and View" application (Helios-600) or "serial-section" protocol (CrossBeam 550). An In-lens detector or a mix of Inlens + SE2 detectors were used to achieve maximal contrast-to-noise ratio. The voxel sizes of the acquired stacks varied. The values per stack are specified in Table I.

*Image analysis*

The images in each stack were aligned with the alignment tool in MIB.[20] Avizo (Thermo Fischer Scientific, version 9.4), Amira (Thermo Fischer Scientific, version 2019.4)

and ImageJ (ImageJ, US National Institute of Health, Maryland, USA) using the plug-in "Linear stack alignment with SIFT" (US National Institutes of Health, Bethesda, Maryland, USA).[21] Contrast enhancement was obtained with the "Enhance Local Contrast" plug-in of ImageJ. "Gaussian Blur 3D" was used as noise reduction filter. Edges sharpening for 3D Visualization was done with the "Unshapr Mask" filter of JmageJ. A 3D presentation and movies were prepared in Amira on the aligned, filtered and contrast enhanced data. The schematic of the proposed model was produced using the educationally licensed Autodesk Maya 2018.

## Results

**Figure 1** is an image of an adult *C. acicula* showing both the soft parts that can be seen through the thin elongated cone-shaped shell. The sealed end, the protoconch, is the first formed shell and hence the thickest part of the shell.[8] The shell thickness of the protoconch is ~12 μm. New shell is formed
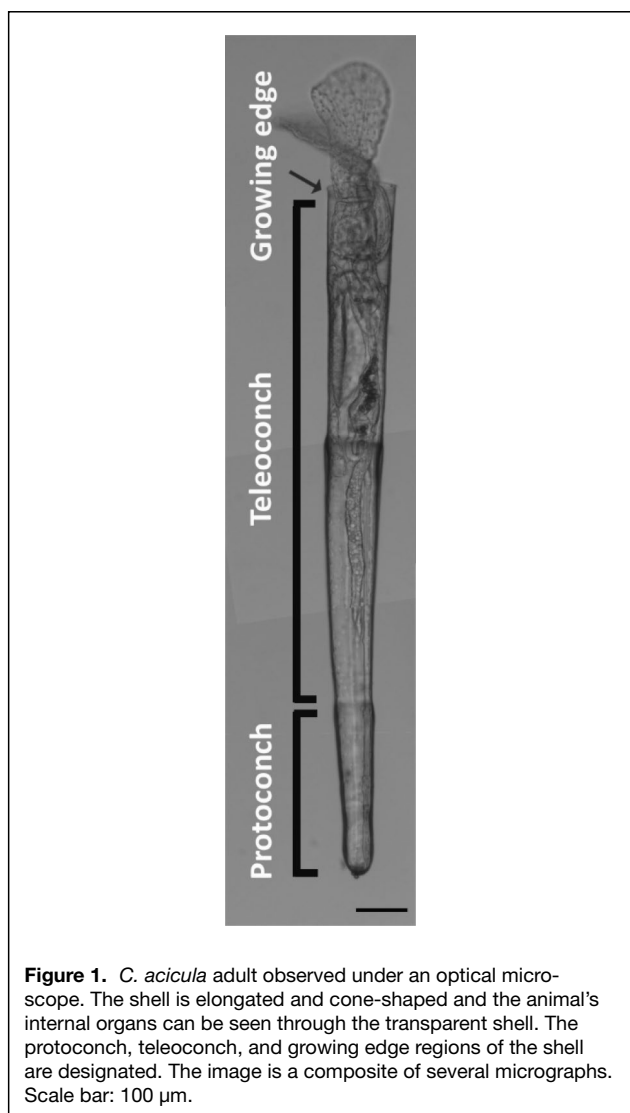


**Figure 1.** *C. acicula* adult observed under an optical microscope. The shell is elongated and cone-shaped and the animal's internal organs can be seen through the transparent shell. The protoconch, teleoconch, and growing edge regions of the shell are designated. The image is a composite of several micrographs. Scale bar: 100 μm.

at the growing edge, where the thickness is ~300 nm.[15] The teleoconch is the shell formed after the larva transforms into an adult.

### Shell microstructure of C. acicula using SEM

SEM images of fracture surfaces through the shell of *C. acicula* contain a wealth of detailed information that has for the most part been observed before in other Cavoliniodea.[6,13,14,16–18,22] (**Figure 2**). The basic building blocks of the structure are aragonitic crystal fibers. When these fibers are viewed on a fracture surface that is more or less parallel to the outer shell surface, many of the fibers are curved, and they are densely packed into arrays (Figure 2a). The fiber sections are often rectangular (Figure 2b). Note too that the individual fiber components of the arrays are not well aligned (Figure 2b). A lower magnification view through the shell section confirms that the fiber arrays have slightly different orientations within a layer, and that the fracture plane in different layers intersects fibril arrays in totally different orientations (Figure 2c). A fractured section through the thick teleoconch region, close to the protoconch, shows many layers of fibril arrays, and the orientations of these arrays in different layers are clearly offset (Figure 2d). Figure 2e shows the interlocking mosaic structure of the fibers. A low magnification view of a long section perpendicular to the long axis of the shell shows that layers of fibril arrays persist across most of the fracture (Figure 2f). In addition, the outer prismatic layer can be clearly seen in Figure 2f. However, based on these SEM images, and the hundreds of others that we have obtained, as well as those that have been published, we were not able to define any consistent 3D structure. Nor did we ever see a complete helical structure.

### Characterizing the preferred orientation of the aragonite crystals using x-ray diffraction

X-ray diffraction patterns were obtained from a shell fragment of a region close to the growing edge (**Figure 3**). The x-ray beam was first oriented parallel to the shell surface (Figure 3a) and then perpendicular to the shell surface (Figure 3b). The beam sampled an area of around 100 μm in diameter. Diffraction patterns obtained from other regions of the shell (teleoconch and protoconch (data not shown)) were very similar to those shown in Figure 3. The diffraction patterns taken with the beam parallel to the shell surface have sharp reflections with well-delimited arcs, showing that the aragonite crystals are well ordered and the crystallographic orientations have preferred alignment. The (002) reflections confirm that the *c*-axes of the aragonite crystals are aligned perpendicular to the shell surface.[14,16,18] In contrast, the diffraction patterns taken with the x-ray beam perpendicular to the surface show no preferred crystallographic alignment of the *a* and *b* aragonite axes in the planes parallel to the shell surface. This is in part due to the fiber curvature, as the *b*-axes are aligned with the fiber long axes,[14,18] and could also be due to the offsets of even closely associated fibers, as seen for example in the inset in Figure 2d. Similar observations were made by Li et al.[14] and by Suzuki et al.[13]
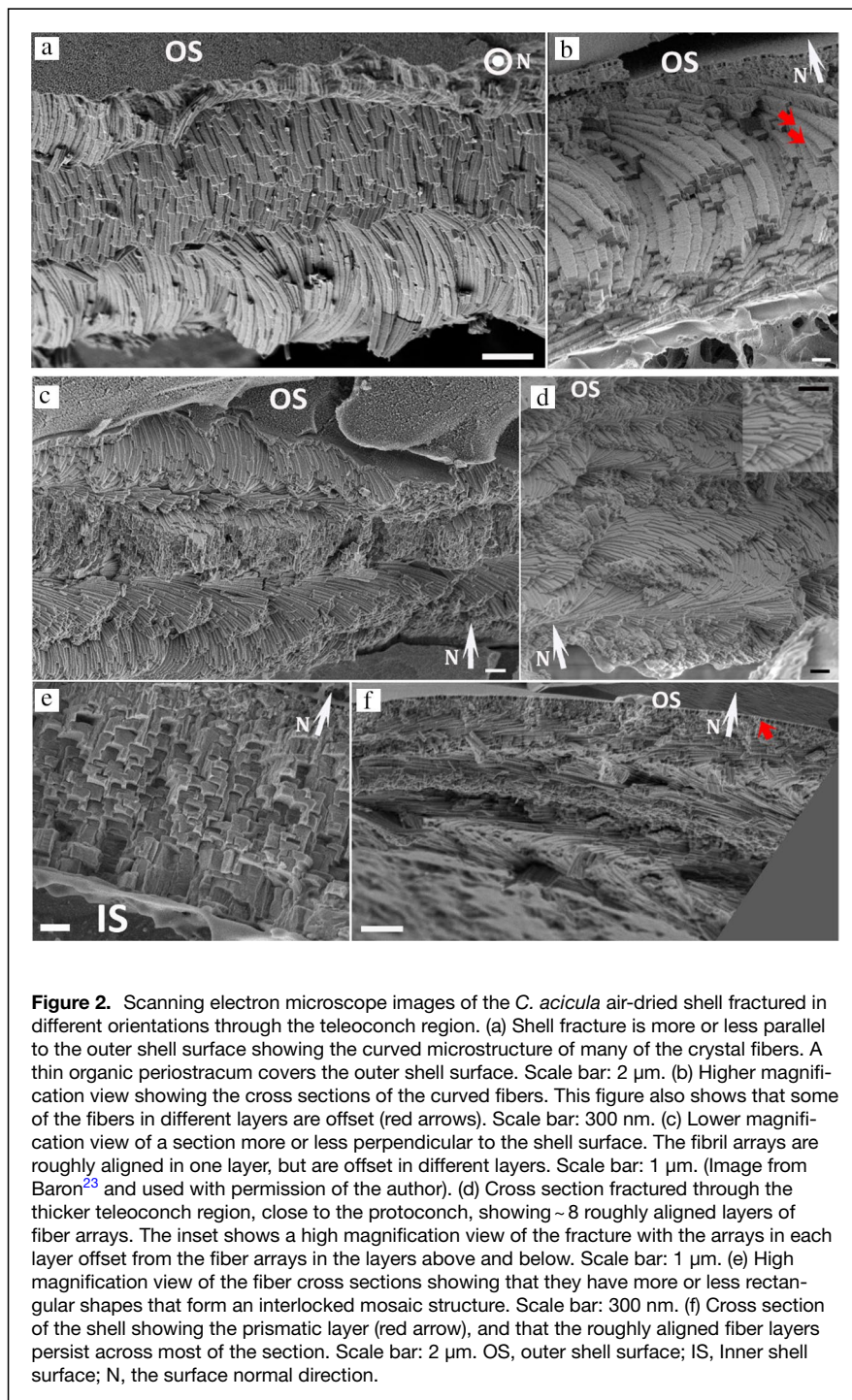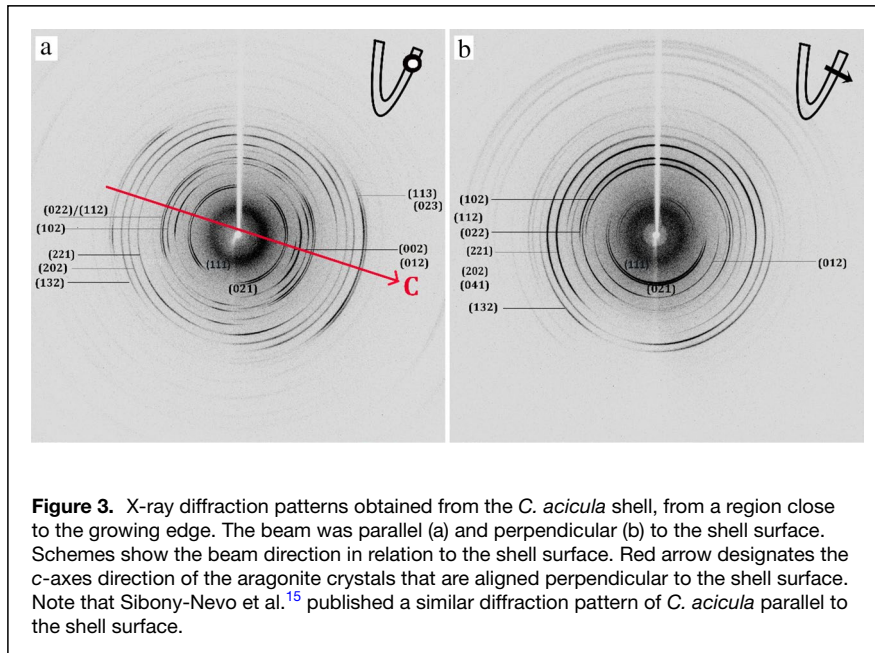
**Figure 2.** Scanning electron microscope images of the *C. acicula* air-dried shell fractured in different orientations through the teleoconch region. (a) Shell fracture is more or less parallel to the outer shell surface showing the curved microstructure of many of the crystal fibers. A thin organic periostracum covers the outer shell surface. Scale bar: 2 µm. (b) Higher magnification view showing the cross sections of the curved fibers. This figure also shows that some of the fibers in different layers are offset (red arrows). Scale bar: 300 nm. (c) Lower magnification view of a section more or less perpendicular to the shell surface. The fibril arrays are roughly aligned in one layer, but are offset in different layers. Scale bar: 1 µm. (Image from Baron[23] and used with permission of the author). (d) Cross section fractured through the thicker teleoconch region, close to the protoconch, showing ~ 8 roughly aligned layers of fiber arrays. The inset shows a high magnification view of the fracture with the arrays in each layer offset from the fiber arrays in the layers above and below. Scale bar: 1 µm. (e) High magnification view of the fiber cross sections showing that they have more or less rectangular shapes that form an interlocked mosaic structure. Scale bar: 300 nm. (f) Cross section of the shell showing the prismatic layer (red arrow), and that the roughly aligned fiber layers persist across most of the section. Scale bar: 2 µm. OS, outer shell surface; IS, Inner shell surface; N, the surface normal direction.

## Three-dimensional structure using FIB-SEM

We initially assumed that to obtain contrast in the FIB-SEM we must use heavy metals to stain the organic matrix. We therefore prepared stained specimens embedded in Epon (**Figure** 4a) and using the FIB-SEM, we could visualize the shell texture (Figure 4b). However, we showed using thin lamellae of the stained shell prepared by FIB-SEM and then examined in the TEM (**Figure** S1), that we were visualizing only the aragonite crystals in Figure 4b and c, and not the stained matrix. **Figure** S1 shows no staining of the organic phase between the crystal fibers. In addition, the difference in contrast of one fiber to another is due to the change in the crystal orientation and not attributed to sample staining (**Figure** S1). This we confirmed using an untreated shell specimen (Figure 4d–e). Based on these observations, we collected seven different stacks from two different specimens at different locations in the shell (Table I). The most informative stacks in terms of better understanding the overall structure are the lower resolution stacks (more than 20-nm slice thickness) that encompass a larger volume. Here we analyze such a stack in detail (Stack B; Table I, Figure 4b–c). We also produced a high resolution stack (10-nm slice thickness) of a smaller volume that shows the individual crystal fibers (Stack G, Table I).

In order to better understand the crystal fiber 3D organization in relation to the shell surface, we define three orthogonal planes: (1) the outer shell surface, (2) the plane perpendicular to the outer shell surface but parallel to the longitudinal axis of the animal (longitudinal plane), and (3) the plane perpendicular to the natural outer shell surface and transverse to the longitudinal axis of the animal (transverse plane) (**Figure** 5). As the original slicing direction is not exactly parallel to the outer surface, the image stack was re-sliced in Avizo, such that the stack was aligned as close as possible to being parallel to the natural outer surface, and hence also to the inner growth surface of the shell.

We conclude that neither SEM images of fracture surfaces nor x-ray diffraction patterns can provide all the information necessary for determining the 3D structure of this shell. We therefore developed the capability to examine this structure in 3D using FIB-SEM. The structure proposed should however be consistent with the information obtained using SEM and x-ray diffraction.

**Figure 3.** X-ray diffraction patterns obtained from the *C. acicula* shell, from a region close to the growing edge. The beam was parallel (a) and perpendicular (b) to the shell surface. Schemes show the beam direction in relation to the shell surface. Red arrow designates the *c*-axes direction of the aragonite crystals that are aligned perpendicular to the shell surface. Note that Sibony-Nevo et al.[15] published a similar diffraction pattern of *C. acicula* parallel to the shell surface.

### Stack B parallel to the outer shell surface

This 3D data set was obtained about 310 μm from the growing edge (Figure 4a, black arrow Stack B; Table I for more details). **Video 1** shows all 421 images obtained sequentially from the outer surface to the inner surface. Note that the thin (<0.5 μm) prismatic layer at the shell surface is not well imaged. In each image below the prismatic layer there are areas in which the fibers are more or less aligned in one direction and areas where they are curved. However, it is impossible to trace an individual fiber across the whole field of view in any of the images. We therefore deduce that the fibers are not only changing directions with increasing distance from the outer surface, but are tilted out of the plane of the natural outer surface.

Figure 6 shows seven different images from this stack with increasing distance from the outer surface. Note that in Figure 6a, close to the outer surface but below the prismatic layer, the linearly aligned fibers are offset by about 20° from the "north–south" direction of the image. In Figure 6b, this offset increases to about 45°, and in Figure 6c the offset is about 90°. This trend continues, and in Figure 6d the fibers are offset by about 135°, and then about 170° (Figure 6e). The rotation of the fibers continues to about 200° (Figure 6f) with increasing distance from the outer surface. Figure 6f–g shows that the fibers begin to curve back in the opposite rotation direction. This continuously changing fiber direction at one location creates an impression of continuity in **Video 1** that reveals a basic structural motif of aligned and curved fibers that are not in the same plane as the outer shell surface, and change direction with increasing distance from the outer surface. In order to gain more insight into the 3D structure, we examine the same stack that was digitally re-sliced in the longitudinal direction (i.e., perpendicular to the outer and inner surfaces and parallel to the long axis of the animal) (**Figure 7**).

### Images parallel to the longitudinal cross section

Figure 7 shows a representative view of the longitudinal section, and **Video 2** shows all the images through the stack in this plane. The longitudinal section can be divided arbitrarily into three zones. A thin top zone (Figure 7, Zone 1) is the prismatic layer in which most of the crystals appear to be almost perpendicular to the natural surface, and to have a different orientation from the underlying layer in Zone 2. In Zone 2, the crystal outlines are less well defined than in Zone 1 and in Zone 3 below. We do not know the reason for this. One possible explanation is that the crystals are oriented out of the longitudinal plane (Figure 7, Zone 2). In Zone 3, the crystal fibers are well defined and appear to follow an S-shaped pathway. Note that the horizontal line near the top of Zone 3 is an imaging artifact. The same motif is preserved through the entire stack and the relative proportions of these zones barely change through the stack (**Video 2**). Careful examination of individual fibers shows that an individual crystal fiber cannot be traced through the whole section implying that the longitudinal section also does not intersect the S-shaped fibers in the plane of the "S."

For completeness we also reconstructed the images in the transverse plane and compared them to an SEM fracture surface in that plane (**Figure** S2). This view of the structure did not provide any new insights.

In order to be sure that Stack B is representative of the structure, we also reconstructed the 3D volume of Stack A after cropping to an X, Y, and Z volume of 13 × 9 × 11 μm, respectively. **Video S1** shows a video of this stack, first with the original images along the milling direction, and then we use a volume rendering mode to better highlight the crystal fiber trends. We do observe the same overall structure as in Stack B, with the outer micron or so below the shell surface comprising the prismatic layer, and below that the arrays of curved fibers observed in different directions. We noted that in some directions the bulk of the crystal fibers seem to be aligned in a plane that is oblique to the shell surface. We therefore examined the possibility that we could identify a surface in which the S-shaped crystal fibers are more or less continuous in a plane oblique to the natural shell surfaces. In order to do this, we continued with Stack B.
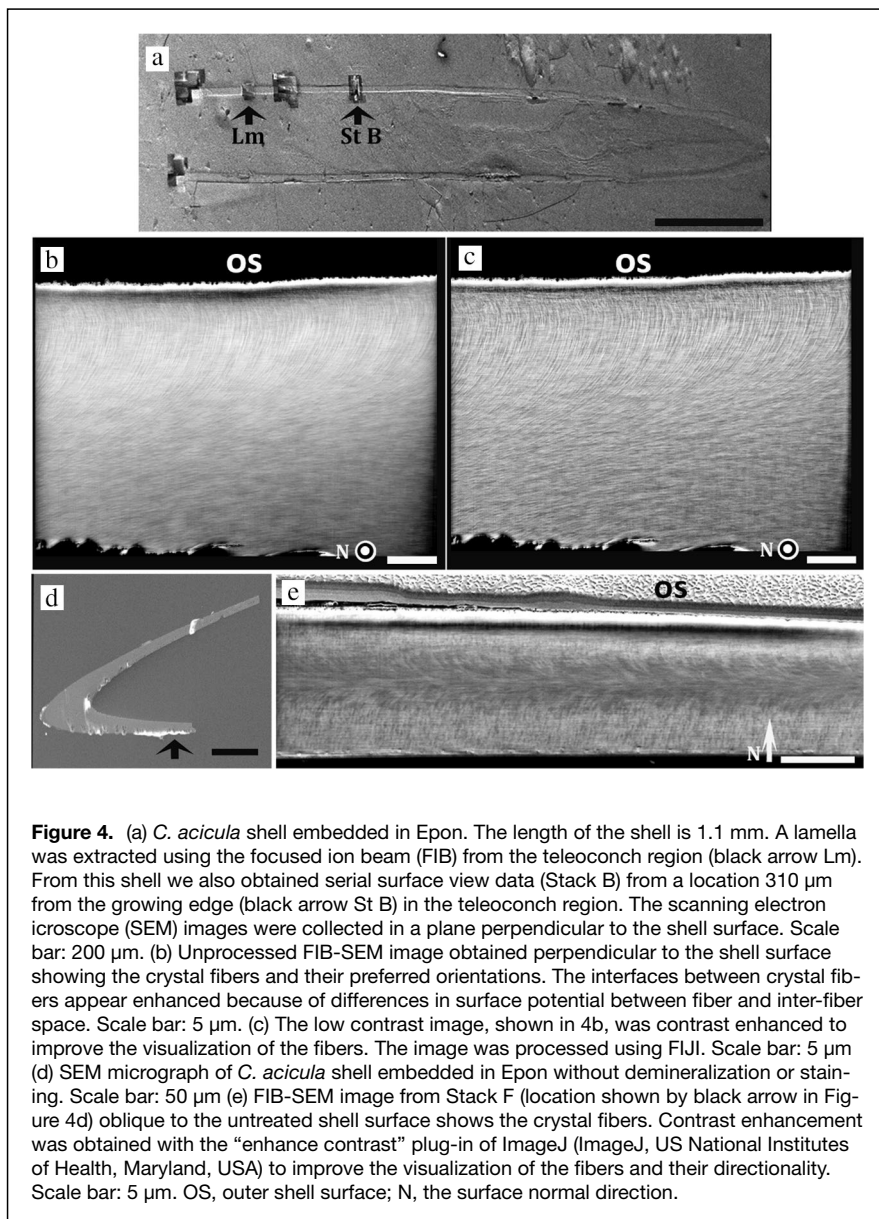
**Figure 4.** (a) *C. acicula* shell embedded in Epon. The length of the shell is 1.1 mm. A lamella was extracted using the focused ion beam (FIB) from the teleoconch region (black arrow Lm). From this shell we also obtained serial surface view data (Stack B) from a location 310 μm from the growing edge (black arrow St B) in the teleoconch region. The scanning electron icroscope (SEM) images were collected in a plane perpendicular to the shell surface. Scale bar: 200 μm. (b) Unprocessed FIB-SEM image obtained perpendicular to the shell surface showing the crystal fibers and their preferred orientations. The interfaces between crystal fibers appear enhanced because of differences in surface potential between fiber and inter-fiber space. Scale bar: 5 μm. (c) The low contrast image, shown in 4b, was contrast enhanced to improve the visualization of the fibers. The image was processed using FIJI. Scale bar: 5 μm (d) SEM micrograph of *C. acicula* shell embedded in Epon without demineralization or staining. Scale bar: 50 μm (e) FIB-SEM image from Stack F (location shown by black arrow in Figure 4d) oblique to the untreated shell surface shows the crystal fibers. Contrast enhancement was obtained with the "enhance contrast" plug-in of ImageJ (ImageJ, US National Institutes of Health, Maryland, USA) to improve the visualization of the fibers and their directionality. Scale bar: 5 μm. OS, outer shell surface; N, the surface normal direction.

### Images in an oblique section

We reoriented the volume sampled, and by re-slicing we reconstructed the structure in oblique planes. We did find an oblique direction crossing all orthogonal planes that reveals a structural motif in which individual fibers appear more or less continuous. This oblique plane intersects the longitudinal plane at an angle of 15° to the shell surface, and by an angle of 25° to the transverse plane. **Figure 8** is a representative image of this plane, and **Video 3** shows all the images parallel to this plane. A roughly continuous S-shaped structure can be seen in all the images in this plane. We conclude that the basic structural motif of this shell, in a plane oblique to the natural surface, is a series of nested aragonite fibers that are curved into

an S shape. **Figure 9** shows a high resolution image from Stack G over a limited area of this oblique surface, in which the individual crystals are clearly continuous through the part of the S-shaped arrays that can be seen in Figure 8. **Video S2** is a video showing the 3D structure of this entire stack including the original images, and then showing these images in the volume rendering mode from different directions. The volume rendering mode highlights better the overall organization of the crystal fibers.

### Discussion

Using FIB-SEM serial block face imaging, we show that in *C. acicula*, the aragonite fibers are organized within the shell volume in 2D planes consisting of nested S-shaped arcs. These 2D planes are oblique to the outer shell surface and intersect the outer shell surface at an angle of 25 degrees. **Video 3** shows images parallel to this plane at different depths. There are no major shifts of the S-curved arrays in one plane relative to the next. We thus conclude that the 2D arrays are more or less superimposed upon each other to form a 3D structure.

The high resolution Stack G (Figure 9) shows that at least some of the fibers in the oblique plane are continuous. There are no obvious discontinuities of the fibers in this plane, which would be present if the top part of the image belongs to one spiral of the helix and the bottom part to another spiral. If the curvature of the fibers in Figure 9 is part of a helical structure, this would imply that the helix axis would be approximately parallel to the shell surface, whereas the helical models published depict the axis as more or less perpendicular to the shell surface.[18] In addition if the curvature is part of a helix, then the diameter of the helix should be around 12 μm and part of the helix should be visible in all the stacks studied. We do not see a helical structure. Finally, **Video S1** shows that in some orientations the fibers appear straight. We do not know if the fibers are actually straight or the nested array of S-shaped fibers are being viewed edge-on. Either way, this feature of the stack is not consistent with a helical structure.
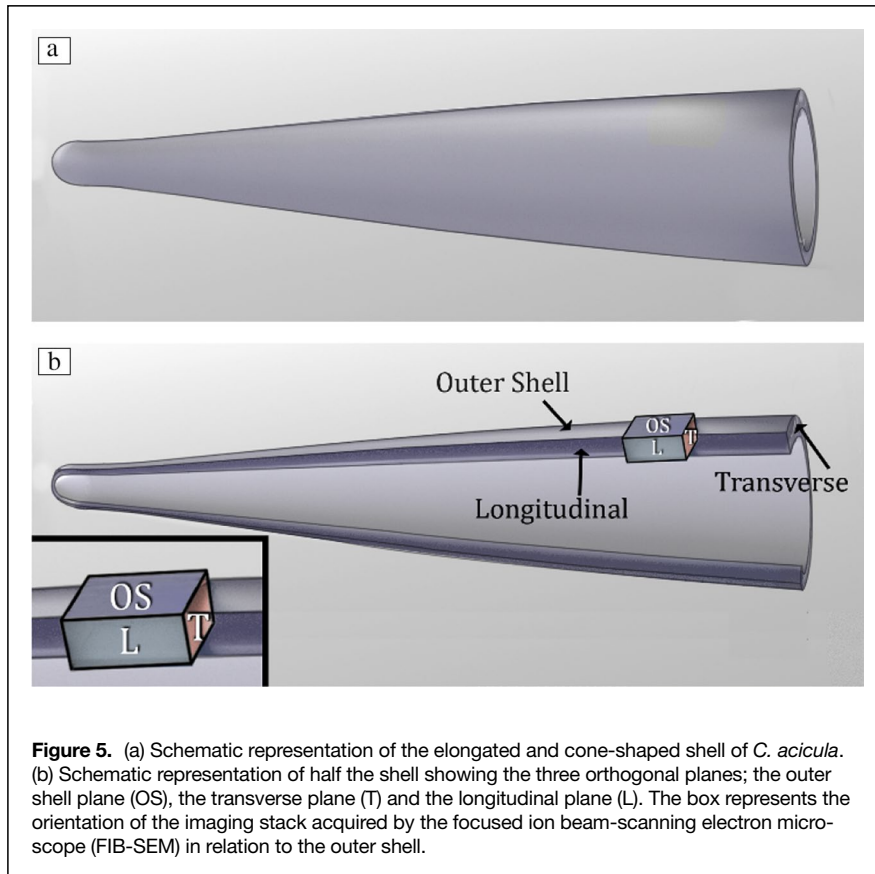
**Figure 5.** (a) Schematic representation of the elongated and cone-shaped shell of *C. acicula*. (b) Schematic representation of half the shell showing the three orthogonal planes; the outer shell plane (OS), the transverse plane (T) and the longitudinal plane (L). The box represents the orientation of the imaging stack acquired by the focused ion beam-scanning electron microscope (FIB-SEM) in relation to the outer shell.
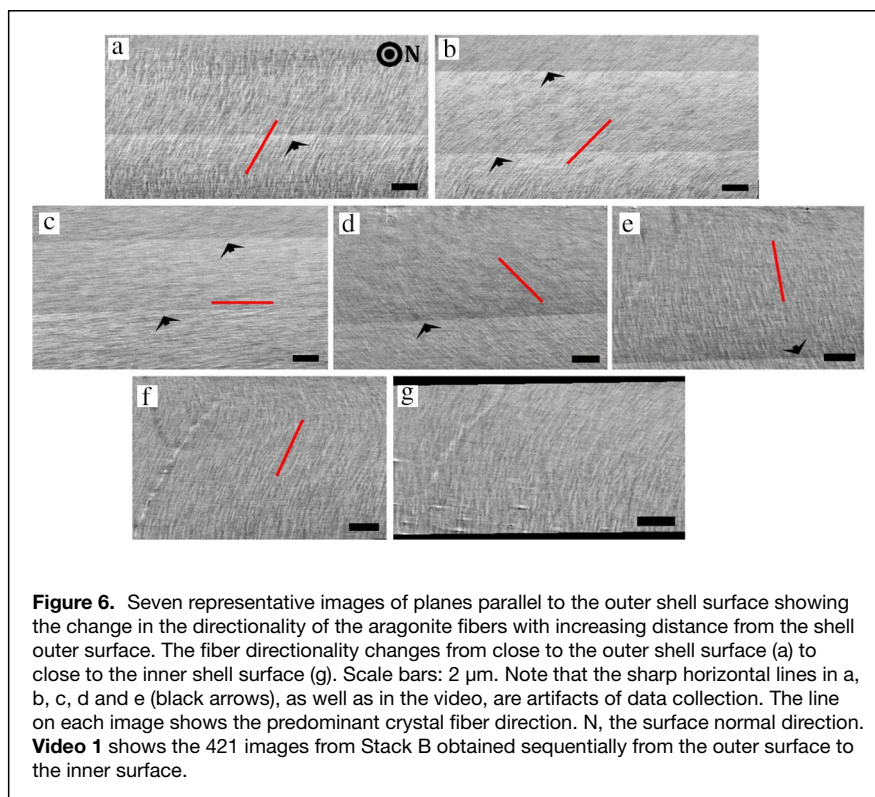


**Figure 6.** Seven representative images of planes parallel to the outer shell surface showing the change in the directionality of the aragonite fibers with increasing distance from the shell outer surface. The fiber directionality changes from close to the outer shell surface (a) to close to the inner shell surface (g). Scale bars: 2 μm. Note that the sharp horizontal lines in a, b, c, d and e (black arrows), as well as in the video, are artifacts of data collection. The line on each image shows the predominant crystal fiber direction. N, the surface normal direction. **Video 1** shows the 421 images from Stack B obtained sequentially from the outer surface to the inner surface.

We emphasize that we have only studied thin parts of the shell using FIB SEM. We do not know if thickening occurs by continuous extensions of the S-shaped linear arrays in the third dimension. We note that in thicker parts of the shell closer to the protoconch, the fracture surface reveals several discrete layers (Figure 2f is a good example). It is possible that the apparent layers are due to the whole 3D array of nested curves shifting to form these layers. It is however also possible that in the thicker part of the shell additional motifs occur that do not exist in the thinner and younger part of the shell.

One question is whether this 3D structure is consistent with the SEM fracture surface observations and the x-ray diffraction patterns? SEM fracture surfaces are not smooth (Figure 2) and so it is almost impossible to reliably follow one crystal fiber from the outer surface to the inner surface. Therefore interpreting a 3D structure based on this rough 2D surface is difficult. The roughness of the fracture is in itself an indication of how the interlocking fibers arranged in arrays limit the ability of cracks to propagate easily through the structure, thus increasing its toughness.[14,16] **Figure** S3 is an SEM image of a shell, in the teleoconch region, that was fractured by chance in such a way as to show approximately orthogonal planes below the outer shell surface. Although one crystal fiber cannot be traced from the outer surface to the inner surface, we think that the overall view of this fracture surface is consistent with the presence of an embedded oblique plane comprising nested arrays of S-shaped crystals.

Our x-ray diffraction patterns are consistent with previous studies in that the *c*-axes of the aragonite fibers are reported to be perpendicular to the shell surface.[13,18] However, as the shell is curved and not flat, it is conceivable that the
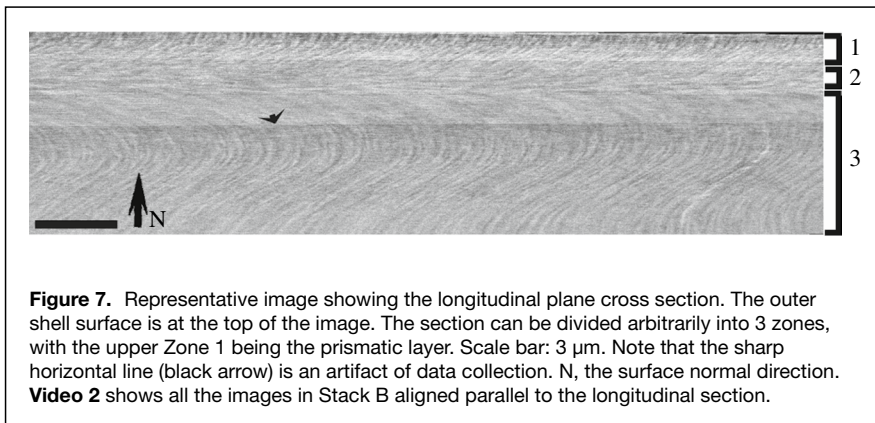
**Figure 7.** Representative image showing the longitudinal plane cross section. The outer shell surface is at the top of the image. The section can be divided arbitrarily into 3 zones, with the upper Zone 1 being the prismatic layer. Scale bar: 3 µm. Note that the sharp horizontal line (black arrow) is an artifact of data collection. N, the surface normal direction. **Video 2** shows all the images in Stack B aligned parallel to the longitudinal section.
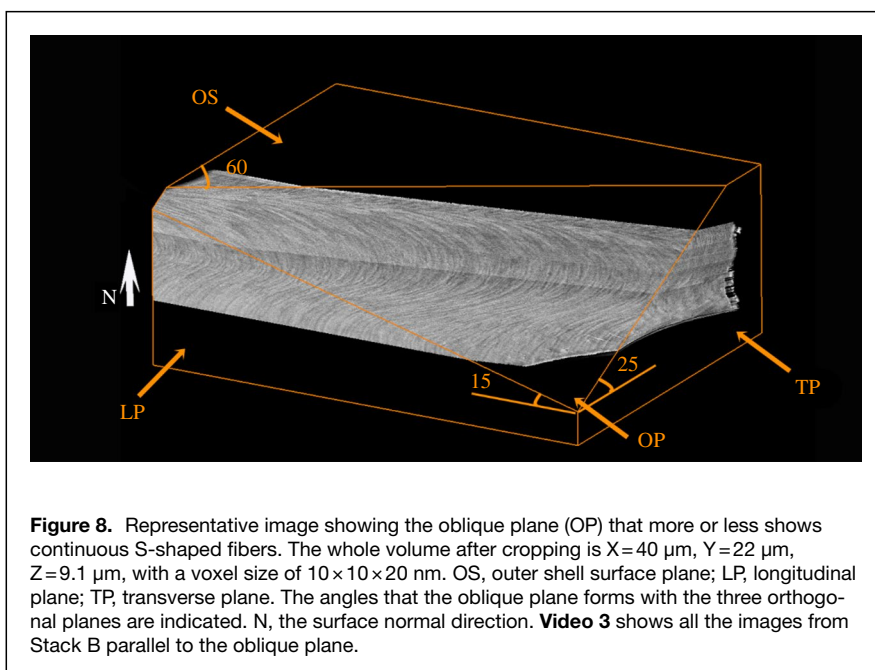


**Figure 8.** Representative image showing the oblique plane (OP) that more or less shows continuous S-shaped fibers. The whole volume after cropping is X = 40 µm, Y = 22 µm, Z = 9.1 µm, with a voxel size of 10 × 10 × 20 nm. OS, outer shell surface plane; LP, longitudinal plane; TP, transverse plane. The angles that the oblique plane forms with the three orthogonal planes are indicated. N, the surface normal direction. **Video 3** shows all the images from Stack B parallel to the oblique plane.

*c*-axes may be perpendicular to the inclined plane in which the nested arcs are located. This plane is inclined approximately 25° from the shell outer surface. The continuous twinning of the crystals in each fiber, observed in previous studies,[14,18] is consistent with the lack of crystallographic alignment of the *a* and *b* aragonite axes.

**Figure** 10a is a schematic drawing showing how an S-shaped curved individual crystal fiber (Figure 10a) can be arranged into a planar nested array (Figure 10b). Two-dimensional layers superimpose to form a 3D structure (Figure 10c), in which the crystals are not exactly aligned as has been observed in SEM micrographs (Figure 2). When this 3D structure is fractured at different locations, crystal fibrils can be exposed edge-on, or at oblique angles (Figure 10d) producing fracture sections that closely resemble the SEM fracture surfaces seen in Figure 10e. Slight disorder was introduced

into the model in the fiber alignment (2°) between stacked 2D planes to better reflect the offsets observed in Figure 2.

Since the initial study of Bé et al.,[6] all subsequent structural studies of Cavolinioidea shells have proposed variants of a helical structure.[13,14,16,18] The structure that we identified is based on the crystal fibers having an S shape and that they are arranged in 2D to form a flat surface. This structure is significantly different from a helical structure. In general, it is difficult to conceive how a helical structure can both maintain its helicity and be totally space filling. Here we propose a possible solution to this conceptual problem by showing that the *Creseis acicula* shell structure is composed, at least in the thin teleoconch region, of 2D arrays of S-shaped fibers that in 3D are slightly misaligned to form a space filling 3D structure.

We also note that in a study of the forming shell of *Cuvierina*, Willinger et al.[18] noted that the crystal fibers emerge from the surface at an angle in relation to the surface plane. This is in agreement with the oblique alignment of the 2D planes in relation to the shell surface. In this arrangement, we would expect the tips of the forming crystals to protrude at an angle to the natural surface.

Shelled pteropods are divided into two main superfamilies; the Cavolinioidea and the Limacinoidea. The Limacinoidea form the most common shell microstructure in gastropods, namely the crossed lamellar microstructure.[11] It is interesting to note that the basic building block of the crossed lamellar structure is a small elongated straight aragonite crystal fiber with thicknesses in the range of around 0.2 µm.[12] The basic building block of the Cavolinioidea, including *C. acicula* studied here, is also an elongated aragonite crystal fiber, with fiber thicknesses usually ranging 0.2–0.3 µm,[4,10–12] This suggests that the Cavolinioidea shell structure is evolutionarily derived from the crossed lamellar structure, but instead of having straight arrays of crystals, the crystal arrays, at least in the case of *C. acicula*, have an S-shaped curvature. This is in agreement with the fact that the limacinid, *Heliconoides mercinensis*,[24] is the assumed ancestor of the two superfamilies of shelled pteropods,[25] and has a crossed lamellar structure. It is intriguing to understand why this complex and unique
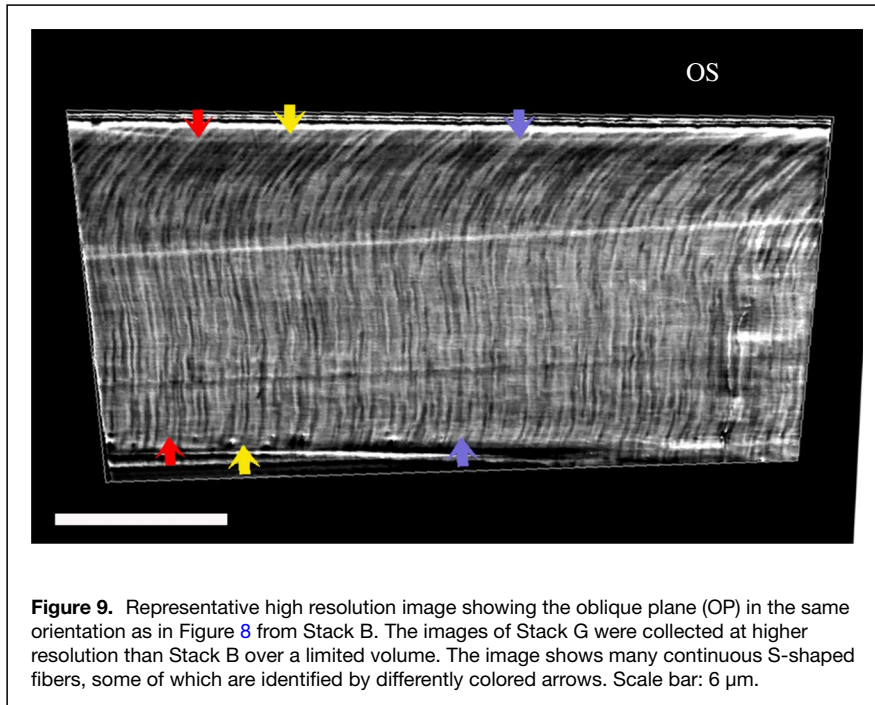
**Figure 9.** Representative high resolution image showing the oblique plane (OP) in the same orientation as in Figure 8 from Stack B. The images of Stack G were collected at higher resolution than Stack B over a limited volume. The image shows many continuous S-shaped fibers, some of which are identified by differently colored arrows. Scale bar: 6 μm.
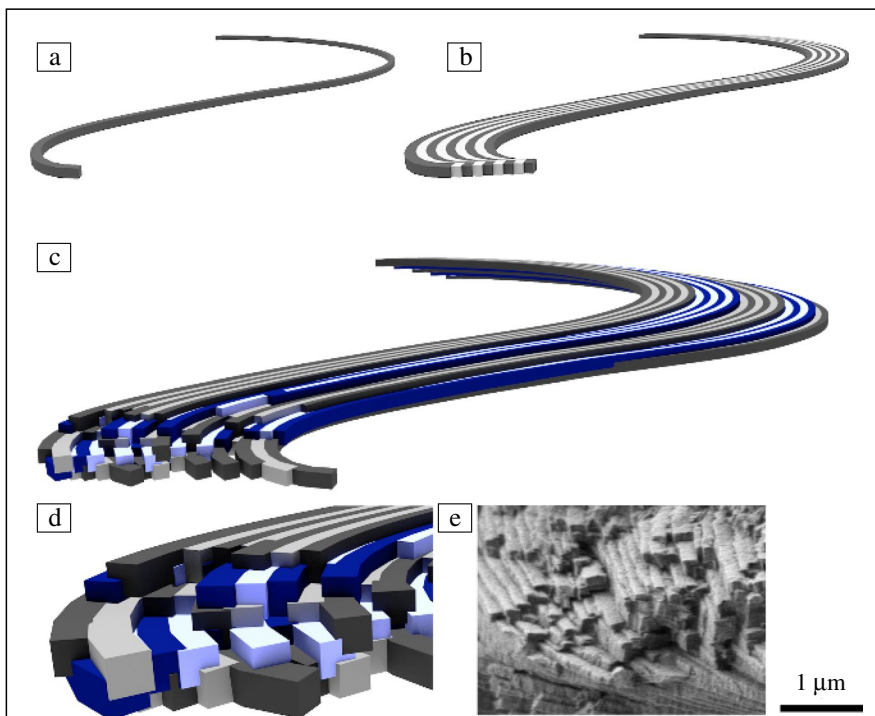


**Figure 10.** Schematic representation of the S-shaped nested aragonite crystal fiber arrays in the oblique plane. (a) An S-shaped curved individual crystal fiber as identified in the oblique plane. (b) A planar array of nine S-shaped crystal fibers nested together. (c) Three-dimensional organization of the S-shaped aragonite fibers. Five planar surfaces of S-shaped arcs are stacked on top of each other and "fractured" at different locations. Crystal fibers can be exposed edge-on, or at oblique angles producing fracture sections. (d) Higher magnification view of the "fracture" surface. (e) Fracture surface showing interlocking microstructures as seen in the scanning electron microscope (Figure 2e) that resemble Figure 10d. Slight disorder was introduced in the fiber alignment (2°) to better reflect the offsets between layers observed in Figure 2. Fibers are colored to better differentiate between different fibers.

S-shaped shell microstructure appeared only twice in the phylogenetic tree, in heteropods and shelled pteropods from the Cavolinioidea superfamily.

## Summary

We show that FIB-SEM serial block face imaging can be used to image the 3D structure of the shell of the pteropod *C. acicula* even without fixing or contrast agents. We analyzed the structure of the thinner, younger part of the shell to obtain structural information on a relatively large volume, and at high resolution (around 10 nm) to observe individual crystal fibers. We show that the repeating unit is a continuous S-shaped crystal fiber organized into nested arrays in a plane oblique to the natural surface. These nested arrays are stacked one on top of another with small offsets to form the 3D structure of one layer.

## Acknowledgments

## Data availability

The data sets generated during and/or analyzed during the current study are available from the corresponding author on reasonable request.

## Ethical approval

None of the material has been published or is under consideration elsewhere, and that all co-authors are aware of and have approved the submission.

## Supplementary Information

The online version contains supplementary material available at https://doi.org/10.1557/s43577-021-00184-3.

## References

1. O. Boggild, *The Shell Structure of the Mollusks* (A.F. Host, Kjobenhavn, Denmark, 1930)
2. J.G. Carter, G.R. Clark, in Mollusks. *Notes for a Short Course*, T.W. Broadhead, Ed. (University of Tennessee, Department of Geological Science Studies, 1985), pp. 50
3. F. Marin, N. Le Roy, B. Marie, *Front. Biosci.* **4**, 1099 (2012)
4. J.G. Carter, *Skeletal Biomineralization: Patterns, Processes and Evolutionary Trends* (Van Nostrand Reinhold, New York, 1990)
5. G. Glaçon, J. Rampal, D. Gaspard, D. Guillaumin, T.S. Staerker, "Thecosomata (pteropods) and Their Remains in Late Quaternary Deposits on the Bougainville Guyot and the Central New Hebrides Island Arc," in *Proceedings of the Ocean Drilling Program Scientific Results* (1994), p. 319
6. A.W.H. Bé, C. MacClintock, D.C. Currie, *Biomineralization Res. Rep.* **4**, 47 (1972)
7. R.L. Batten, M.P. Dumont, *Bull. Am. Mus. Nat. Hist.* **157**, 263 (1976)
8. A.W.H. Bé, R.W. Gilmer, "Zoogeographic and Taxonomic Review of Euthecosomatous Pteropoda," in *Oceanic Micropaleontology*, A.T.S. Ramsay, Ed. (Academic Press, London, UK, 1977), vol. 1, p. 733
9. S. van der Spoel, *Euthecosomata, A Group with Remarkable Developmental Stages (Gastropoda. Pteropoda)* (Zoological Museum, Amsterdam, The Netherlands, 1967)
10. W. Sato-Okoshi, K. Okoshi, H. Sasaki, F. Akiha, *Polar Biol.* **33**, 1577 (2010)
11. C. Salinas, D. Kisailus, *JOM* **65**, 473 (2013)
12. K. Bandel, in *Skeletal Biomineralization: Patterns, Processes and Evolutionary Trends*, J. G. Carter, Ed. (Van Nostrand Reinhold, New York, 1990), p. 117
13. M. Suzuki, T. Sasaki, Y. Oaki, H. Imai, *Cryst. Growth Des.* **17**, 191 (2016)
14. L. Li, J.C. Weaver, C. Ortiz, *Nat. Commun.* **6**, 6216 (2015)
15. O. Sibony-Nevo, I. Pinkas, V. Farstey, H. Baron, L. Addadi, S. Weiner, *Cryst. Growth Des.* **19**, 2564 (2019)
16. T. Zhang, Y. Ma, K. Chen, M. Kunz, N. Tamura, M. Qiang, J. Xu, L. Qi, *Angew. Chem.* **123**, 10545 (2011)
17. A.G. Checa, E. Macías-Sánchez, J. Ramírez-Rico, *Sci. Rep.* **6**, 25989 (2016)
18. M.G. Willinger, A.G. Checa, J.T. Bonarski, M. Faryna, K. Berent, *Adv. Funct. Mater.* **26**, 553 (2015)
19. A.W. Janssen, *Basteria* **82**, 110 (2018)
20. I. Belevich, M. Joensuu, D. Kumar, H. Vihinen, E. Jokitalo, *PLoS Biol.* **14**, e1002340 (2016)
21. J. Schindelin, I. Arganda-Carreras, E. Frise, V. Kaynig, M. Longair, T. Pietzsch, S. Preibisch, C. Rueden, S. Saalfeld, B. Schmid, *Nat. Methods* **9**, 676 (2012)
22. K. Bandel, *Biomineralization Res. Rep.* **9**, 73 (1977)
23. H. Baron, *Characterization of Shell Microstructures and the Shell-Tissue Interface of Shelled Pteropods from Cavoliniidae Family* (Weizmann Institute of Science, Rehovot, Israel, 2014)
24. A. Watelet, T. Lefèvre, *Ann. R. Soc. Malacol. Belg.* **15**, 100 (1885)
25. A.W. Janssen, K.T.C.A. Peijnenburg, in *The Mediterranean Sea: Its History and Present Challenges*, S. Goffredo, Z. Dubinsky, Eds. (Springer, Dordrecht, The Netherlands, 2014), p. 341